RSC Advances

RSC Advances

www.rsc.org/advances

ROYAL SOCIETY OF CHEMISTRY

www.rsc.org/advances

In vitro model reaction of sulfur containing bio-relevant ligands with Pt(II) complex: Their kinetics, mechanism, bioactivity and computational studies

Subhajit Mukherjee[a], Venkata P. Reddy B.[a], Ishani Mitra[a], Rajnarayan Saha[a], Jagadeesh C Bose K[b], Subba Reddy Dodda[b], Wolfgang Linert[c] and Sankar Ch. Moi[*a]

a. Department of Chemistry, National Institute of Technology, Durgapur-713209, W.B. India

b. Department of Bio-Technology, NIT Durgapur-713209, W,B, India

c. Institute of Applied Synthetic Chemistry, Vienna University of Technology, Getreidemarkt 9/163- AC, 1060, Vienna, Austria

∗Author for correspondence, email: sankarmoi67@yahoo.com

This submission was created using the RSC Article Template (DO NOT DELETE THIS TEXT)

(**LINE INCLUDED FOR SPACING ONLY - DO NOT DELETE THIS TEXT**)

Abstract

Cis-[Pt(MAMP)Cl$_2$] **1** and its hydrolysed product cis-[Pt(MAMP)(H$_2$O)$_2$]$^{2+}$ **2** (where MAMP = 2-[(N-methylamino) methyl]pyridine) were synthesised and characerised by spectroscopic methods. Kinetic and mechanistic studies were followed on complex **2** with thiols; L-cysteine (L-cys) and N-acetyl-L-cysteine (N-ac-l-cys). The thiol substituted products [Pt(MAMP)(L-cys)] **3** and [Pt(MAMP)(N-ac-L-cys)] **4** formation mechanisms were proposed and characterized. Their bonding modes were also confirmed spectroscopically and theoretically. At pH 4.0, the interactions of complex **2** with the ligands show two distinct consecutive steps: the first step is dependent and the second is independent of [Ligand]. The association equilibrium constant (K_E) for the outer sphere complex formation and rate constants for both steps have been evaluated. The activation parameters ($\Delta H^‡$ and $\Delta S^‡$) for both the steps were calculated using Eyring equation and an associative mechanism is proposed for both the reactions. Structural optimization, HOMO-LUMO energy calculation, Natural Bond Orbital (NBO) analysis of complex **2-4** was investigated with Density Functional Theory (DFT). The complexes bind strongly to DNA and change its electrophoretic mobilization pattern in agarose gel. For theoretical understanding of the binding interaction of complex **2** with B-DNA, molecular docking study was performed. Anticancer property of all the three complexes **2-4** were probed on both HeLa and Hep G2 cell lines which shows remarkable activity of 70-75% compared to cisplatin at 50.0 μM concentration. Significant growth inhibition by the complexes in both gram positive and gram negative bacteria was observed. The water soluble complexes **2-4** may be further investigated and might be considered as chemotherapeutic agent.

Introduction

Cisplatin, [Pt(NH$_3$)$_2$Cl$_2$] is a well known antitumor drug and used for the treatment of cancer throughout the world. However, it is associated with certain toxic properties.[1-3] Several platinum complexes have been synthesized and evaluated for their anticancer activity. However, a few of these complexes have entered clinical trials, of which the following are currently approved: carboplatin[4-7], nedaplatin[8] (in Japan), oxaliplatin.[4,9,10] But these are also not fully devoid of toxic property and their effectiveness is limited to only specific types of cancer. To reduce the toxicity, d^8 metal ion systems, particularly Pt(II) and Pd(II) complexes carrying nitrogen and sulfur containing ligands have been under focus. In vitro adduct formation of Pt(II) complexes with the thiols and thio-ethers finally control platination of DNA[11]. It is believed that binding of Pt(II) complex[12-15] with the thiols is a kinetically favoured biochemical process. The resulting Pt–S (thio-ether/thiols) bond might be terminated in the presence of DNA, i.e. the N^7 atom of 5′-GMP can substitute the thio-ether molecule. Consequently, it is further believed that these Pt–S adducts[16] can act as a drug reservoir in our physiological system before the interaction with DNA, i.e. they are suitable intermediates of the reaction of

Pt(II) complex and DNA. The anticancer property of Pt-S complexes[17] is of current interest to the researchers for their in vitro biological importance. Owing to the high affinity of Pt(II) towards the thiols and their vital role in our physiological system, interactions between complex **2** with L-cys and N-ac-L-cys are considered as model reactions. Generally Pt(II) complexes carrying N and S donor chelates have significant antitumor property[4-7,18]. [Pt(MAMP)(H$_2$O)$_2$]$^{2+}$ **2** has been designed by considering few specific reasons like; Pt(II) complexes having carrier ligand amine and labile groups H$_2$O instead of chlorides (cisplatin) might have anticancer property. Due to labile nature of diaqua complexes, H$_2$O molecules are easily replaceable by S, O and N containing ligands and subsequently substitution reactions are followed. Secondly, the carrier ligands MAMP (2-[(N-methylamino)methyl]pyridine) is a σ-donor and π-acceptor ligand and strongly binds with the metal ion and generally are not substituted by S, O and N containing ligands i.e. inert to substitution process. Again, according to the hypothesis of Y. Kidani and his coworkers[19], the carrier ligand should have at least one amino hydrogen (-NH-CH$_3$), which is responsible for its anticancer property. Therefore, this desired property is also satisfied by the designed complex **2**.

Moreover, the complex **2** is highly water soluble, which satisfies the precondition for being an anticancer drug.
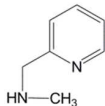
2-[(N-methylamino)methyl]pyridine

In our Laboratory, we have investigated[20,21] the kinetics, mechanism, bioactivity and molecular docking studies of $[M(pic)(H_2O)_2]^{2+}$ (where, M = Pt(II) or Pd(II), pic = 2-Aminomethylpyridine) and it shows significant cytotoxic property near about 70% compared to cis-platin. Herein, we report the synthesis of another complex $[Pt(MAMP)(H_2O)_2]^{2+}$ **2** and detailed kinetics and mechanism for the interactions between complex **2** with L-cys and N-ac-L-cys individually were considered for their importance.

Experimental
Instrumentation
Elemental analysis of the complex **1** was carried out on a Perkin-Elmer 2400 series-II CHNS/O Analyser. Conductivity measurements were performed with a Systronics conductivity meter (Model 308), where the cell constant was calibrated with standard buffer solution. The pH measurements were done with the help of a EUTECH digital pH meter (pH Tutor) with accuracy of ±0.01 U, calibrated with a Standard phosphate buffer solution (KH_2PO_4/Na_2HPO_4). Fourier Transform infrared (FTIR) spectra of the complexes were recorded on a Nicolet-iS-10 spectrometer (KBr disk, in the range of 4,000–400 cm^{-1}). The kinetic measurements were conducted at pH 4.0 on a Shimadzu UV 1800 spectrophotometer attached to a thermoelectric cell temperature controller (Model TCC-100, accuracy ±0.1 ^0C). The pK_a values of the complex **2** were determined by titro-processor (Metrohm, 888 Titrando). NMR spectra were recorded with a Bruker Avance-400 and 200 (400 MHz and 200 MHz) spectrometer using D_2O or DMSO-d_6 as solvent. ESI Mass spectra were carried out in Waters Q-TOF Micro YA263 Mass spectrometer in water.

Computational details
The pKa values of the complex **2** were determined by tiamo 2.4 software package. All geometry optimization and energy calculations were performed using Density Functional Theory (DFT) at the B3LYP[22,23] level of theory for the complexes **2**-**4** implemented in Gaussian09 software programme package[24]. Global minimum optimized structures were confirmed by frequency analysis at the same level of theory. The relativistic effective core potential (ECP) and associated valence double ξ(zeta) basis set of Hay and Wadt[25,26] (LANL2DZ) were employed for Pt atom. This comprises of electrons in the 6s, 6p, and 5d orbitals. The standard split valence basis set 6-31G(d)[27,28] was applied for carbon, oxygen, nitrogen, hydrogen and sulfur. The NBO[29] analysis was performed to get insight electronic structure and bonding of the complexes **3**-**4**. HEX 8.0.0 software was used for molecular docking of complex **2** with B-DNA (PDB ID: 1BNA).

Reagents and methods
All chemicals used for the kinetic and bio-activity study were of highest purity as available. The starting compounds K_2PtCl_4 (99%), 2-[(N-methylamino) methyl]pyridine (MAMP) (97%), L-cysteine (97%), N-acetyl-L-cysteine (98%), $AgClO_4$ (97%) and $AgNO_3$ (99%) were purchased from Sigma Aldrich. Potassium dihydrogen orthophosphate and $NaClO_4$ were purchased from Merck. All these reagents were used without further purification. For kinetic purpose, double distilled water was used to prepare all kinds of solutions and molecular biology grade water was used for bioactivity study. All solvents used were of analytical grade. To investigate the bioactivity, Human cervical carcinoma (HeLa) and hepatocellular carcinoma (Hep G2) cell lines were cultured in DMEM medium (Hi-Media) containing 10% FBS (Hi-Media) with antibiotic concentration 1% of penicillin/streptomycin (50 IU ml^{-1} and 500 mg ml^{-1}) respectively in CO_2 incubator with a humidified atmosphere (95% air and 5% CO_2) at 37 ^oC for 2 days. Cell viability was studied using MTT (3-(4,5-dimethylthiazolyl-2)-2,5-diphenyltetrazoliumbromide) colorimetric assay based on a reaction between enzyme dehydrogenase of mitochondria from viable cells with the yellowish colour tetrazolium rings moiety of MTT. The colour can be quantified by using the colorimetric assay on a multi-well scanning spectrophotometric method by ELISA reader (Stat Fax™® 2100 Micro plate Reader, USA). Bright field inverted microscope (Zeiss) was used to detect the survival cells of HeLa and Hep G2 cell lines.

Job's method of continuous variation was carried out to confirm the Metal : Ligand (M : L) ratio for the reactions between complex **2** with L-cys and N-ac-L-cys separately at pH 4.0. The complex **2** and the ligand were mixed according to their possible different ratios, like 1:1, 1:2, 2:1 etc and heated to near about 50 ^oC for few hrs and absorbances were measured until or unless reached to maximum. The exact M : L ratio was found with proper calculation and shows a bell shaped curve when absorbance vs [M]/[M]+[L] was plotted. The development of a characteristic peak in the product complexes **3** and **4** at 259 nm and 261 nm respectively were monitored as a function of time at different fixed temperatures.

Molecular docking of complex **2** with B-DNA (PDB ID: 1BNA) was done using HEX 8.0.0 software. Hex calculates DNA-complex binding, assuming that the complex is rigid and it superposes pairs of molecules using the knowledge of 3D shape only. It uses a spherical polar fourier (SPF) correlations to accelerate the calculations. In order to run the docking protocol in HEX, first DNA and ligand in PDB format were loaded. By clicking on the control option in main menu, Docking was selected and activated. The parameters which were used in the docking process are listed in ESI Table S1. The results obtained after

the docking process was analysed. The E-Total values of the complex against DNA were calculated. To validate the procedure and results we had run the same protocol three times and obtained almost same results. Relative RMSD values were calculated and it is lower than 2Å.

Syntheses of complexes
[Pt(MAMP)Cl$_2$] 1

The complex [Pt(MAMP)Cl$_2$] **1** was prepared from K$_2$PtCl$_4$ (0.25 g, 0.6 m.mol), dissolved in requisite amount of water and the solution was heated to 40-50 ^{o}C. Ligand MAMP dissolved in minimum volume of water was added dropwise into the K$_2$PtClO$_4$ solution. The reaction mixture was stirred with magnetic stirrer for overnight at 40 to 50 ^{o}C fitted with reflux condenser and a light yellow precipitate of [Pt(MAMP)Cl$_2$] appears and the solution becomes colourless due to completion of the reaction. The mixture was then allowed to cool and the precipitate was filtered off and washed with water, acetone and diethyl ether. The precipitate was dried in vacuum desiccator and the dry weight was found to be 0.187gm (0.48 m.mol; yield 80%) of complex **1**. Elemental analysis of complex **1**(C$_7$H$_{10}$N$_2$Cl$_2$Pt) gave; C= 20.39% (21.65); H= 2.36% (2.60) and N = 6.75% (7.22) where the numbers in parentheses were calculated from the chemical formula. Electronic absorption spectrum of **1** in DMF, (λ_{max}/nm) ($\mathcal{E}$/M^{-1}cm^{-1}): 310(5035). Selected IR frequencies (KBr disk, cm^{-1}): 3159(s), 3034(s), 2923(s), 2848(s), 1654(s), 1617(s), 1559(m), 1448(m), 1282(s), 1156(s), 1085(s), 835(b), 721(m), 663(s) and 498(s) (ESI Fig. S1).

^{1}H NMR. (200 MHz, DMSO-D$_6$) of complex **1** (δ in ppm and J in Hz): δ 9.16 (d, J = 6.0, 1H^a), δ 8.15 (t, J=8.0, 8.0, 1H^c) δ 7.68 (d, J=8.0, 1H^d), δ 7.51 (t, J= 6.0,8.0 1H ^{b}), δ 4.2 (m, J=6.0, 2H^e), δ 2.74 (m, d, H^f) and δ 2.52 (d, J=4.0 , 3H^g) (ESI Fig. S2).

^{13}C NMR. (200 MHz, DMSO-D$_6$) of complex **1**(δ in ppm) (SI Fig.): C^h (163.23); C^a (147.38); C^c (139.01); C^d (124.44); C^b (122.41); C^g (62.59) and C^e (39.0; m)(ESI Fig. S3).

[Pt(MAMP)(OH$_2$)$_2$](ClO$_4$)$_2$ 2

The diaqua complex, [Pt(MAMP)(OH$_2$)$_2$](ClO$_4$)$_2$, **2** was prepared in solution by the method of Hay and Basak[30]. The chloro complex [Pt(MAMP)Cl$_2$], **1** (0.15 g; 0.38 m.mol) was converted into the diaqua complex **2** in solution by adding two equivalents of AgClO$_4$ solution. Great care was taken to remove Ag$^+$ ions. To ensure the complete removal of Ag$^+$ ion from the solution a slightly less amount of AgClO$_4$ (0.1576 g; 0.760 m.mol) was taken than the calculated amount (0.1602 g; 0.773 m.mol) for complete utilization of Ag$^+$ to remove the chlorides from diaqua complex **2**. It was kept overnight and the AgCl precipitate was removed by filtration through a special pressure drive membrane (pore size 0.05 mm, GFC) filter (ultra filtration). The slight amount of chloro complex, remained unchanged was removed along with the AgCl precipitate. The concentration of complex **2** solution

was calculated on the basis of consumed amount of AgClO$_4$. To check the presence of eventual remaining of Ag$^+$ is done by adding dil HCl and no precipitate was found. To ensure that no trace of Ag+ ion remained in the solution, the pH was adjusted to 12–13 and the black Ag$_2$O precipitate was filtered off. The pH of the complex **2** solution was adjusted at 3.0 to prevent dimerisation and freshly prepared dilute solutions of the same were used for kinetic measurements. Another aliquot of complex **2** was prepared from **1**, as NO$_3^-$ salt [Pt(MAMP)(H$_2$O)$_2$](NO$_3$)$_2$ using AgNO$_3$ solution for hydrolysis (same method as AgClO$_4$) for the purpose of bioactivity studies. Electronic absorption spectrum of **2** in water, (λ_{max}/nm) ($\mathcal{E}$/M^{-1}cm^{-1}): 271(5946). Selected IR frequencies (KBr disk, cm^{-1}): 3541–3456(br), 3425(s), 3111(s), 2928(s), 1657(s), 1614(s), 1482(s), 1448(s), 1144(br), 1088(s), 827(b), 721(m), 626(s) and 491(s) (ESI Fig. S4). ^{1}H NMR (400 MHz, D$_2$O and DMSO-D$_6$) of complex **2** (δ in ppm and J in Hz): δ 8.48 (d, J = 5.6, 1H^a), δ 8.4 (t, J=5.6, 3.2, 1H^c) δ 7.98 (d, J=6.0, 1H^d), δ 7.85 (t, J= 5.2,4.8 1H ^{b}), δ 4.2 (s, 2H^e), δ 2.76 (m, H^f) and δ 2.87 (d, 3H^g)(ESI Fig. S5)
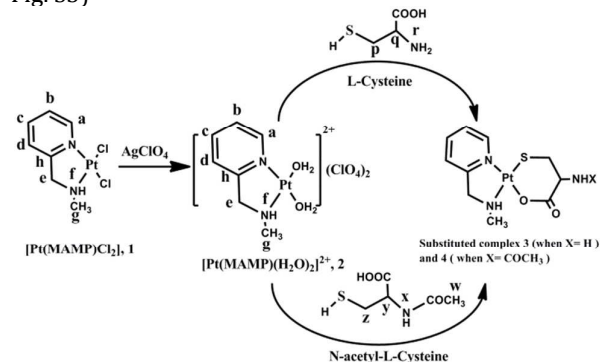
Structures of Complexes and Ligands

Syntheses of complex 3 and 4

Thiols (L-cys and N-ac-L-cys) substituted product complexes [Pt(MAMP)(L-cys)] **3** and [Pt(MAMP)(N-ac-L-cys)] **4** were synthesized by mixing L-cys and N-ac-L-cys separately with complex **2** in 1 : 1 molar ratio at pH 4.0 respectively. The complex **3** was characterized by electronic absorption spectrum in water λ_{max}/nm ($\mathcal{E}$/M^{-1} cm^{-1}): 259 (7042); selected IR frequencies (KBr disk, cm^{-1}): 3424(b), 3231(br), 3056(br), 1735(br), 1617(s), 1546(s),1480-1421(b), 940(s), 767(s), 626(s), 452(s) and 425(s) (ESI Fig. S6). ^{1}H NMR (400 MHz, DMSO-D$_6$) data for complex **3**: δ 8.6 (d, J = 3.6, 1H^a), δ 7.91 (t, J = 1.6, 4.8, 1H^c), δ 7.48 (d, J = 6.0, 1H^d), δ 7.44 (t,2.0, 4.0, 1H^b), δ 4.29 (s, 2H^e), δ 2.54 (d, J= 4.4,3H^g), δ 2.53 (m, 1H^f), δ 2.75 (d,d, J= 3.6, 6.0 2H^p) and δ 2.50 (t, J= 1.6, 1.2, 1H^q) (ESI Fig. S7). ESI-mass spectrum of **3** shows important peaks at m/z 218.95, 314.87, 437.86(100%, molecular ion peak) in water (ESI Fig. S8).

Electronic absorption spectrum of **4** in H$_2$O λ_{max}/nm ($\mathcal{E}$/M^{-1} cm^{-1}): 261 (9603); selected IR frequencies (KBr disk, cm^{-1}): 3404(br), 3233(br), 3058(br), 1734(b), 1654-1612(b), 1541(s), 1473-1413(b), 1375(s), 1143(s), 940(s), 769(s), 626(s),

424(s) and 418(s) (ESI Fig. S9). ^{1}H NMR (400 MHz, δ in ppm, DMSO-D$_6$) data: δ 8.65 (d, J = 3.6, 1H^a), δ 8.26 (t, J = 7.2, J = 6.4, 1H^c), δ 7.72 (d, J = 6.0, 1H^d), δ 7.47 (t, J = 6.4, J = 6.4, 1H^b), δ 4.3 (s, 2H^e), δ 2.5 (m, 2H^f), δ 2.88 (s, 3H^g); δ 1.85 (s, 3H^w); δ 7.93 (d, J = 5.2 1H^x), δ 2.76 (m, J= 3.2 2H^z) (ESI Fig. S10). ESI-Mass spectrum of **4** shows important peaks at m/z 266.85, 314.84, 437.85 and 500.77 in water. (ESI Fig. S11)

Synthesis safety note

Perchlorate salts of transition metals should be handled cautiously as these are hazardous and explosive upon strong heating. To hydrolyse the chloro complex, we have used 0.76 m.mol of silver perchlorate solution and dilute solution (maximum concentration 9.1242× 10^{-3} M) of perchlorate salt of Pt(II) complexes were used for kinetic and analysis purpose. The hydrolysis process does not involve any heating, hence there was no possibility of explosion. For kinetic study, maximum temperature was 45 ^{o}C, which is not too high temperature. Appropriate safety precautions were used while handling the salt. No explosion event was encountered in the present study.

Determination of pK$_a$ values of complex 2

The pKa values of the complex **2** were determined by potentiometric measurement using Metrohm Titrando-888 titro-processor with standard 0.05 M KOH solution using tiamo 2.4 software package. The electrode and titro-processor were calibrated with standard buffer solutions prepared according to NBS specifications. pK$_a$ values were measured by pH versus volume titration (Fig. 1) of 3.04×10^{-3} (M) complex **2** and the ionic strength was adjusted to 0.1 M with NaClO$_4$, at 25 ^{o}C. The pH was plotted against volume of base consumed. The relationship pH–p[H] = 0.05 was observed. Two equivalent points EP1 and EP2 were observed in the titration curve corresponding to the pKa values as HP1 and HP2. The pKa$_1$ and pKa$_2$ values of complex **2** were found to be 4.83 and 6.72 respectively, which are comparable with the reported pK$_a$ values of almost similar system[31] [Pt(pic)(H$_2$O)$_2$]$^{2+}$ complex.
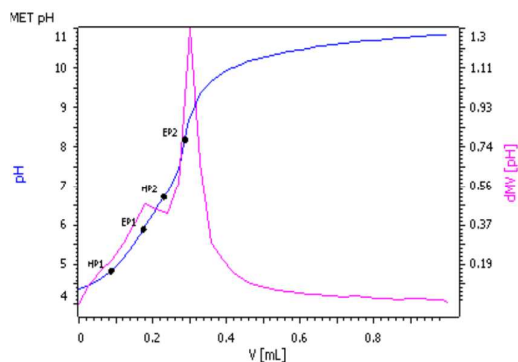
Fig. 1 pH vs volume (mL) of 0.05M KOH solution

Kinetic investigation

For kinetic study, the standard mixing technique was followed and pseudo-first-order reaction conditions were employed for all the kinetic runs. The progress of the reactions was followed by measuring the increase in absorbance at 242 nm and 245 nm, where the spectral difference between the complex **2** and the product complexes **3** (Fig.3) and **4** (ESI Fig. S12) respectively is at a maximum. Plots of ln(A$_α$- A$_t$) versus time, where A$_α$ and A$_t$ are the absorbances at infinite time (after completion of the reaction) and at time t respectively, for the interaction of ligands (L-cys or N-ac-L-cys) with complex **2** were found to be nonlinear (Fig. 2) at the initial stage and subsequently of constant slope. This indicates that the reaction proceeds via two consecutive steps. From the limiting linear portion of the curve, values of k$_{2(obs)}$ were obtained. The k$_{1(obs)}$ values were obtained from plots of ln Δ versus time (where, Δ is the difference of X-Y part of initial curvature (within 5 mins) (Fig. 2, Inset). Origin software was used for computational analysis. Weyh and Hamm method[32] was adopted to calculate the rate constants for both the two consecutive steps. The rate data, represented as an average of duplicate runs, are reproducible within ±4%.
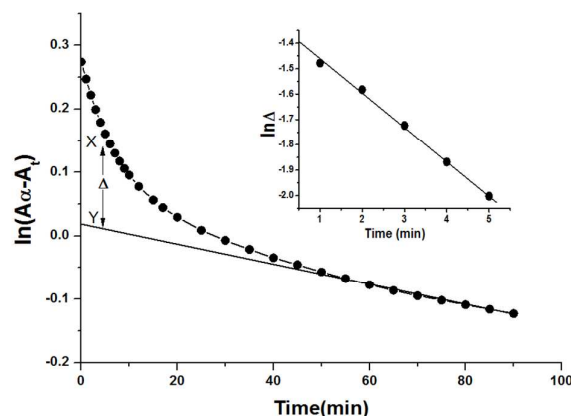
Fig. 2 A typical plot of ln(A$_α$ - A$_t$) versus time (min): [complex **2**] = 3.04× 10^{-4} M; [L-cys] = 3.04× 10^{-3} M; temperature = 25 ^{o}C; Inset: typical plot of ln Δ vs time (min)

Bioactivity study

In vitro antibacterial assay

Antibacterial activity of complex **2** and thiol (L-cys and N-ac-L-cys) substituted complexes **3** and **4** were studied on both the gram positive (Bacillus subtilis) and gram negative (E. coli Dh5a) model organisms.

Tube dilution method for antibacterial activity

Tube dilution method was performed by determining the minimum inhibitory concentration (MIC) and minimum bactericidal concentration (MBC) for antimicrobial activity of complexes **2-4**. The set of 10 sterile tubes were prepared by dispensing the LB broth medium in each tube to attain desired volume. The blank and control were maintained for each setup. These tubes were distributed with appropriate volume of Pt(MAMP) complexes **2-4** from the 1 μM stock solution of tested compound. The final concentration of the complexes ranges from 5.0 μM to 50.0 μM. 10 ml of diluted bacterial suspension was immunized to each tube to give a final concentration of 5×10^5 CFU ml^{-1}.

The same steps were carried out for three sets with appropriate blank and incubated at 37 °C at 120 rpm for 12 hours. Optical density was measured at 600 nm which indirectly represents the number of cells in each tube. Tetracycline was used as a positive control (data not shown). All tests were performed in triplicate and minimal bactericidal growth was determined as inhibition by observing the absorption pattern in LB broth. The average values of the absorbance by Escherichia coli DH5a and Bacillus subtilis at 600 nm were considered and % of growth inhibition was calculated and Graph Pad Prism software was used to plot the graph.

Direct DNA interaction studies of Pt(II) complex 2-4 by agarose gel electrophoresis

Aliquots of 1–3 mg of plasmid PcDNA3 containing complex **2** and the other L-cys and N-ac-L-cys substituted complexes **3** and **4** respectively, were used for this study. Complexes **2**-**4** were directly incubated with plasmid DNA in a final volume of 20 ml for 10 min at 37 °C. The reaction was terminated by the addition of 5 ml loading buffer consisting 0.25% bromophenol blue, 0.25% xylene cyanol FF and 30% glycerol in water. The plasmids were analyzed in 1% agarose gel.

Anticancer property

Cells and culture conditions

HeLa and Hep G2 cell lines were used in this investigation. The cells were grown in DMEM (Hi-Media) containing 10% FBS (Hi-Media) and 1% of penicillin/streptomycin (50 IU ml^{-1} and 500 mgml^{-1}) and cultured for two days at 37 °C in 5% CO$_2$ incubator.

***In vitro* cytotoxicity assay**

Cell viability was investigated by the MTT colorimetric assay.[33,34] Approximately 10,000 cells in DMEM medium were added to each well of a 96-well plate. After 24 h of incubation, the cells were treated with desired concentration (5-50 μL) of Pt(MAMP) complexes and cis-Platin [Cisgland from Gland Pharma Limited] was used as positive control.[35] The plates were incubated for 48 to 72 h. After that 20 μL MTT (5 mg ml^{-1} in PBS) solution was added to each well and incubated for another 3 h. 150 μl of DMSO was added to each well to dissolve the blue formazan product. The absorbance of this product was measured at 540 nm, using (Enzyme-linked immunosorbent assay) ELISA plate reader (Stat Fax™® 2100 Microplate Reader, USA).[36]

Results and discussion

Job's analysis

Job's experiment shows metal:ligand (ratio) as 1: 1 for products **3** and **4** (ESI Fig. S13 and S14). Complex **2** and thiols (L-cys and N-ac-L-cys) were mixed accordingly (1 : 1 molar ratio) at pH 4.0 for their characterization and a pale yellow solution was obtained in each case. Substituted products **3** and **4** were dried slowly and solid products were obtained for further spectroscopic analyses.

Spectroscopic analyses

Characterization of **3-4** was carried out by spectroscopic methods and detailed observations are described as follows using UV-Vis, FTIR, ^{1}H NMR, ESI-Mass spectroscopy.

Electronic spectra (UV-Vis). Electronic spectra of L-cys and N-ac-L-cys substituted products **3** and **4** respectively display different λ$_{max}$ values in aqueous medium with hypsochromic as well as hyperchromic shift in both the cases compared to the complex **2**. The spectral changes of the products are due to n → π* and π → π* transitions of their respective ligands in complex **3** and **4**, which indicate the formation of new products. Repetitive scan of complex **3** formation from the mixture of complex **2** and L-cys, shows two distinct isosbestic points, which amply clear that the reaction goes through the formation of intermediate **B** via sulfur coordination of ligand. The final product **C** is formed by the coordination of carboxylate (COO-) oxygen. The Uv-Vis spectrum of product complex **3** possesses two soldering at 155 and 267 nm with λ$_{max}$ at 259 nm (Fig. 3). The spectrum of complex **4** obtained from the reaction of complex **2** and N-ac-L-cys shows λ$_{max}$ at 261 nm.
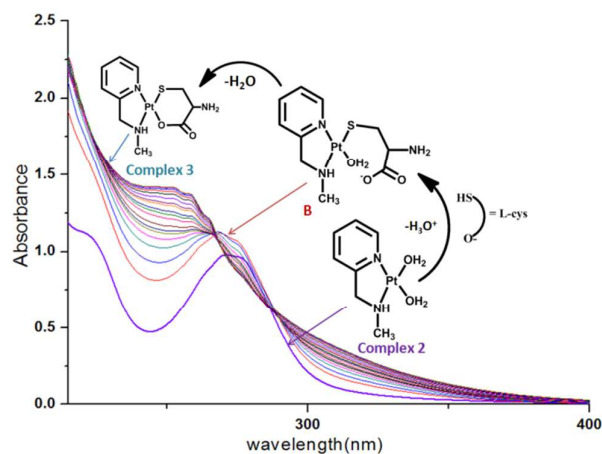
Fig. 3 Transformation of complex **2** to **3** via formation of intermediate **B**

Infrared spectra. The bonding mode of the ligands with complex **2** have the possibility through either (S,O) or (S,N). The characterization of complex **3** and **4** were performed by comparing the IR spectra of the ligands and their respective complex. Sulfur coordination of the thiol group of the first step reaction is predicted according to SHAB principle accompanied by liberation of thiol (S -H) proton and pH decreases from 4.0 to 3.56. This fact is also supported by FTIR spectrum of complex **3**, in which ν_{S-H} str frequency of L-cys at 2540 cm^{-1} disappeared (ESI Fig. S6, S9, S15 and S16).[37–39] ν_{S-H} str. frequency of N-ac-L-cys at 2538 cm^{-1} was also not observed[40] in its corresponding Pt(II) complex **4**, which clearly indicates that sulfur of L-cys and N-ac-L-cys coordinates with Pt(II) centre. Another coordinating site of ligands between carboxylate (COO$^-$) oxygen or

amine (NH_2) nitrogen was confirmed by comparing the str. frequencies of free ligands and their corresponding complexes. The OH stretching bands of the carboxylic group in the free ligands have low intensity, and appear at quite lower frequency 1623 (w) cm^{-1} and split into several components. A couple of strong bands, assigned to $\nu_{as}(COO)$ and $\nu_s(COO)$ appear in the spectra of **3** and **4** at around 1654– 1612 cm^{-1} and 1420–1413 cm^{-1} respectively, as should be expected for a coordinated carboxylate group.[37,38,41] Thus, (S, O) chelation has been suggested for Pt(II) complexes with such ligands.[42] In the substituted products **3** and **4**, ν_{Pt-O} bands appear at 425 & 424 and ν_{Pt-S} band at 452 and 418 cm^{-1} respectively. No change in the position of the strong band $\delta(NH_2)$ around 1617cm^{-1} in **3** and **4** clearly indicates that nitrogen of the amino acids are not ligated to the Pt(II) metal.[43–45] It is very difficult to assign all vibrational frequencies but attempts have been made to specify characteristic frequencies which support the (S ,O) coordination of the ligands in their respective Pt(II) complexes.

^{1}H NMR spectra. The chemical shift position of –NH_2 protons remains almost unaltered at 2.87 ppm in complex **3** as compared to that of L-cys which indicates that –NH_2 is not the coordinating site to Pt(II) centre. However, the position of the thiol proton (–S–H) does not appear in the expected region of 1.5 ppm in the product complex **3**. It clearly provides the evidence of sulfur chelation to Pt(II) followed by change in positions of other protons. More or less similar changes of shift in position of same protons of N-ac-L-cys were observed in complex **4**.

ESI Mass spectra. The ESI-mass spectrum of the complex **3** is shown in ESI Fig. 8. The molecular ion peak at m/z 437.86 corresponds to (Pt(MAMP) + L-cys) which confirms the proposed product to 100% abundance of the isotope peaks matched with the expected values. The other peaks appear at m/z 457.80, 419.83, 314.87 and 218.95. Similarly for complex **4**, peaks are found at m/z 266.85, 314.84, 437.85(major peak) and 500.77 (molecular ion peak, for ([Pt(MAMP)(N-ac-L-cys)] + Na^+)(ESI Fig. S11).

Kinetic study

The ligands (L-cys and N-ac-L-cys) and complexes **2-4** are soluble in water. Thus, the kinetic investigations were performed in aqueous medium. The acid dissociation constants pKa_1 (–COOH) and pKa_2 (–SH) values are 1.71 and 8.35 for L-cys[46] and 3.24 and 9.52 for N-ac-L-cys[47] respectively at 25 ^oC. Both L-cys and N-acetyl-L-cys exist mainly as a neutral species (LH) at pH 4.0. The equilibria are:

$$LH_2^+ \underset{K'_2}{\overset{K'_1}{\rightleftharpoons}} LH + H^+$$
$$LH \rightleftharpoons L^- + H^+$$
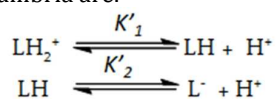
The pKa_1 and pKa_2 values of the complex **2** were found to be 4.83 and 6.72 respectively. Thus at pH 4.0 the reactant complex **2** exists as the diaqua complex ion. At constant temperature, pH 4.0 and fixed concentration of complex **2**, the $ln(A_\alpha - A_t)$ versus time plots (Fig. 2 for

L-cys and SI Fig. S17 for N-ac-L-cys) for different thiol concentrations were curved at the initial stage and subsequently of constant slope. This indicates that the reaction proceeds through a two-step consecutive process and predicts that in the first step, one water ligand from **2** is replaced by the thiol (–SH) group of both L- cys and N-ac-L-cys. The second step is a slow process, where another water ligand is substituted by carboxylate (–COO^-) group leading to ring closure. The rate constant for such a process can be evaluated by assuming the following scheme:

$$A \overset{k_1}{\rightarrow} B \overset{k_2}{\rightarrow} C$$
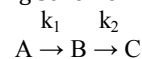
Where, A is the diaqua complex **2**, B is the mono substituted intermediate, and C is the final product **3** or **4**. Formation of C from B is predominant (Fig 3) after some time has elapsed and the rate becomes slower than the first step. The derived rate equation of the reactions based on kinetic observations is as follows,

$$Rate = \frac{K_1 K_E [Thiol]}{1 + K_E [Thiol]} [Complex\ \mathbf{2}] + k_2 [Complex\ \mathbf{2}]$$

Where, K_E = outer sphere association equilibrium constant.

Evaluation of rate constant k_1

The rate constant $k_{1(obs)}$ for the A→B step was evaluated by the method of Weyh and Hamm[31] using the usual consecutive rate law (graphing software was avoided for calculation of k_1, as we know that where the plots show initial curvature, Weyh and Hamm method gives good results. But in other cases, we have used Origin pro 8.0 software for calculations). It shows dependence on ligand concentration. At a definite temperature, the rate constant $k_{1(obs)}$ for the interaction of both the ligands (L-cys and N-ac-L-cys) with the complex **2** were obtained from plots of ln Δ versus time t. Typical plots are shown in Fig. 2(Inset) (ESI Fig. S18 for N-ac-L-cys) and are collected in Table 1. According to SHAB principle sulfur atom of the thiols is good nucleophile towards the Pt(II) centre and substitutes one water molecule in the first step. The rate constants were calculated according to the consecutive rate law of Weyh and Hamm method;

$A_\alpha - A_t = a_1 exp(-k_{1(obs)}t) + a_2 exp(-k_{2(obs)}t)$ (1)

i.e. $A_\alpha - A_t - a_1 exp(-k_{1(obs)}t) = a_2 exp(-k_{2(obs)}t)$ (2)

where, a_1 & a_2 are constants dependent on the rate constant and extinction coefficient. The value of [($A_\alpha - A_t$) - $a_1 exp(-k_{1(obs)}t$)] are obtained from X–Y at different time (Fig. 2) when time is small. So, Δ = $a_1 exp(-k_{1(obs)}t$) or, ln Δ = constant - $k_{1(obs)}t$.

Table 1 $10^3 \times k_{1(obs)}$ (s^{-1}) values at different [L-cys] and [N-ac-L-cys] at different temperatures. [Complex 2] = 3.04×10^{-4} M, pH = 4.0, ionic strength = 0.1 M $NaClO_4$

[L-cys.]$\times10^3$	Temp. (^oC)				
	25	30	35	40	45
3.04	1.42±0.	1.96±0.	2.41±0.	2.79±0.	3.31±0.02

	02	01	04	07	
4.56	1.77±0.05	2.44±0.03	2.97±0.02	3.44±0.03	4.04±0.05
6.08	2.03±0.04	2.79±0.02	3.39±0.07	3.9±0.04	4.54±0.04
7.60	2.22±0.01	3.05±0.05	3.68±0.05	4.22±0.03	4.94±0.06
9.12	2.38±0.06	3.23±0.02	3.89±0.03	4.45±0.02	5.19±0.03
[N-ac-L-cys]×10^3	Temp. (°C)				
	25	30	35	40	45
3.04	1.05±0.01	1.18±0.03	1.38±0.04	1.61±0.07	2.0±0.03
4.56	1.23±0.04	1.37±0.04	1.61±0.03	1.87±0.03	2.3±0.06
6.08	1.35±0.06	1.50±0.02	1.75±0.03	2.02±0.03	2.47±0.03
7.60	1.43±0.05	1.59±0.03	1.86±0.01	2.14±0.02	2.66±0.03
9.12	1.50±0.03	1.66±0.02	1.92±0.03	2.20±0.05	2.75±0.05

The $k_{1(obs)}$ values are derived from the slope of the plot of ln Δ versus time (Fig. 2, Inset) and $k_{2(obs)}$ were calculated from extrapolated part of the linear portion of $ln(A_\alpha - A_t)$ versus time curve at any time 't'. A similar method of calculation was followed for each ligand concentration from $3.04×10^{-3}$ to $9.12×10^{-3}$ M range at constant [complex **2**] ($3.04×10^{-4}$M) at pH 4.0, μ = 0.1 M NaClO$_4$ and at different temperatures 25, 30, 35, 40 and 45 °C respectively. Reaction rate increases with the increase of [thiol] up to a limiting rate (Fig. 4), which is probably due to the completion of outer sphere association complex formation[48,49] followed by interchange of the ligands from the outer sphere to inner sphere, i.e. ligand approaches to the metal centre to form inner sphere complex.
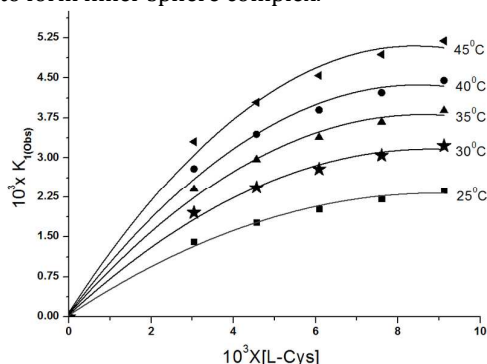
Fig. 4 Plot of $10^3k_{1(obs)}$ versus 10^3[L-cys] from temperature 25 to 45 °C

In the first substitution step of inner sphere complex, one water molecule is replaced by sulfur of the thiol. After completion of this process, the second step is followed by substitution of another water molecule by carboxylate oxygen (-COO$^-$) to form (S,O) chelated final product (C) i.e. complex **3** or **4**. The ligand concentration dependence $k_{1(obs)}$ values can be explained in terms of rapid formation of inner sphere association complex between the reactant complex **2** and the thiol in A→B step. The following scheme can be proposed.

$$\text{complex } \textbf{2} + \text{thiol} \xrightarrow{K_E} \text{complex } \textbf{2}.\text{thiol} \xrightarrow{k_1} \text{B} \xrightarrow{k_2} \text{C}$$
(Inner sphere complex)
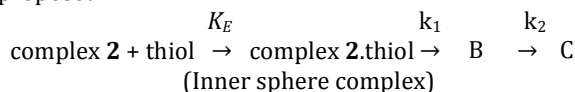
Scheme 1 where, thiol = L-cys or N-ac-L-cys, B = sulfur chelated intermediate, and C = final product (S, O) chelate (**3** or **4**).

K_E is the outer sphere association equilibrium constant and k_1 is the rate constant for the formation of (B).

$d[B]/dt = k_{1(obs)}K_E[A][thiol]/(1+K_E[thiol])$

$d[B]/dt = k_{1(obs)}[A]_T$

Where, subscript T stands for total concentration of complex

Thus it can be written as

$k_{1(obs)} = k_1K_E[thiol]/(1+K_E[thiol])$ (3)

The equation can be written as:

$1/k_{1(obs)} = 1/k_1 + 1/k_1K_E[thiol]$ (4)

The $k_{1(obs)}$ values thus obtained are also dependent on the studied ligand concentration range. However, studies at further higher concentration up to $9.12×10^{-3}$M not follow the linearity (Fig. 4) (ESI Fig. S19 for N-ac-L-cys). The $k_{1(obs)}$ values at different ligand concentration at different temperatures are presented in (Table 1) and $k_{2(obs)}$ are independent of ligand concentration but increases with the increase of temperature (Table 2).

Table 2 $10^5×k_{2(obs)}$ (M^{-1}s^{-1}) values at different [L-cys] and [N-ac-L-cys] at different temperatures [Complex **2**] = $3.04×10^{-4}$M, pH = 4.0, ionic strength = 0.1 M NaClO$_4$

[L-cys]x10^3	Temp.(°C)				
conc	25	30	35	40	45
3.0414	2.81±0.03	3.10±0.01	4.06±0.05	4.32±0.03	5.36±0.05
4.5621	2.78±0.08	3.16±0.05	4.10±0.07	4.32±0.01	5.38±0.06
6.0828	2.81±0.04	3.22±0.03	4.06±0.05	4.34±0.03	5.37±0.04
7.6035	2.81±0.05	3.15±0.04	4.02±0.05	4.30±0.01	5.36±0.02
9.1242	2.85±0.01	3.17±0.06	4.06±0.04	4.32±0.01	5.38±0.01

[N-ac-L-cys]×10³	Temp. (°C)				
conc	25	30	35	40	45
3.0414	2.45±0.02	2.82±0.02	3.27±0.03	3.65±0.04	4.11±0.02
4.5621	2.45±0.03	2.81±0.04	3.27±0.03	3.65±0.02	4.11±0.03
6.0828	2.44±0.01	2.82±0.08	3.27±0.01	3.66±0.03	4.10±0.04
7.6035	2.45±0.01	2.82±0.05	3.27±0.03	3.64±0.01	4.12±0.03
9.1242	2.46±0.04	2.83±0.09	3.27±0.02	3.65±0.01	4.11±0.05

Temp. (°C)	L-cys			N-ac-L-cys		
	$10^3 k_1$ ($M^{-1}s^{-1}$)	K_E (dm^3 mol^{-1})	$10^5 k_2$ (s^{-1})	$10^3 k_1$ ($M^{-1}s^{-1}$)	K_E (dm^3 mol^{-1})	$10^5 k_2$ (s^{-1})
25	3.58±0.10	214.61±0.24	2.81±0.32	1.89±0.08	407.9±0.13	2.45±0.01
30	4.82±0.12	224.51±0.17	3.16±0.26	2.09±0.05	418.99±0.22	2.82±0.03
35	5.64±0.09	244.75±0.18	4.06±0.18	2.39±0.12	453.45±0.16	3.27±0.03
40	6.38±0.15	256.61±0.15	4.32±0.19	2.72±0.09	476.83±0.21	3.65±0.01
45	7.30±0.14	271.85±0.16	5.37±0.28	3.37±0.05	508.24±0.32	4.11±0.03

The plot of $1/k_{1(obs)}$ versus $1/[thiol]$ is found linear (Fig. 5) (ESI Fig. S20 for N-ac-L-cys) with an intercept of $1/k_1$ and a slope of $1/k_1 K_E$. This was found to be so at all temperatures studied. The k_1 and K_E values (Table 3) were obtained from the intercept and from the slope-to-intercept ratios of the same plot respectively.
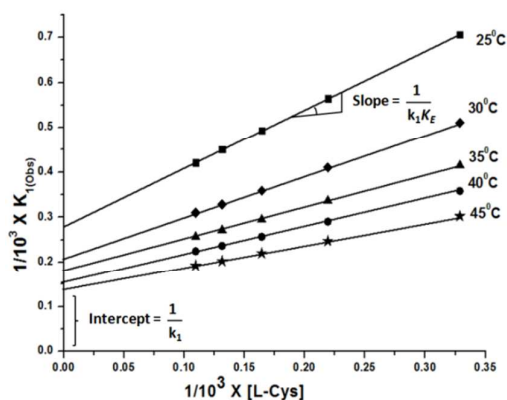
Fig. 5 Plot of $1/10^3×k_{1(obs)}$ versus $1/10^3[L-cys]$ at different temperatures.

Evaluation of rate constant k_2

For the second step reaction, $k_{2(obs)}$ are independent of [thiol] but increases with the increase in temperature (Table 2). The B →C step is assigned to ring closure in which oxygen of carboxylate (–COO⁻) group binds to the metal centre. According to SHAB principle, Pt(II)–oxygen binding is more favourable than Pt(II)–nitrogen of –NH₂ group, and this process is slower than the first step. As the $k_{2(obs)}$ values are independent of [thiol], therefore, the $k_{2(obs)}$ values are equivalent to rate constant k_2 of the second step. At each temperature, the k_2 values were calculated from the limiting linear portion of the $\ln(A_\alpha - A_t)$ versus time curves and are collected in Table 3.

Table 3 Rate constants for the [Pt(MAMP)(H₂O)₂]²⁺ with L-cys and N-ac-L-cys at pH 4.0 and 0.1 M NaClO₄

Effects of pH and temperatures

The reactions were studied at six different pH values. The $k_{(obs)}$ values for both the steps increase initially from pH 3.0 to 4.0 and at higher pH from 5.0 to 7.4 decrease in cases of complex formation **3** and **4** with increase in pH at fixed concentrations of 3.04×10⁻⁴M of [complex **2**], 3.04×10⁻³M of [thiol] and 0.1 M of ionic strength. The $10^3×k_{1(obs)}$ values at 25 °C were 0.89, 1.42, 1.35, 1.21, 1.13 and 0.91 s⁻¹ and $10^5×k_{2(obs)}$ values were 2.44, 2.81, 1.67, 1.48, 1.00 and 0.50 s⁻¹ at pH 3.0, 4.0, 5.0, 6.0, 6.8 and 7.4 respectively for formation of complex **3**. Similar trend is observed in case of complex **4**. The increase in rate may be explained based on the acid dissociation equilibria of the thiols and the complex **2**. In the studied pH range, the complex **2** exists as major diaqua species upto its first pK_{a1} value (4.83). After that the diaqua species transformed to bridging dimer[50,51], which reacts with the thiols comparatively at a slower rate. The rate enhancement upto pH 4.0 might be explained by the deprotonation and increased donor ability of the thiols. At higher pH, the percentage of bridged dimer is maximum, consequently the rate decreases. The characteristic pH dependence for the substitution reaction can be theoretically explained by considering the following derived rate expression:

$$k_{(obs)} = k_a K_a [L]_{Total}/(k_a + [H^+])$$

We have considered COOH as a donor centre where, k_a, K_a and $[L]_{total}$ are the rate constants, acid dissociation constant of the L-cys and N-ac-L-cys's carboxylate groups and total [thiol], respectively. As a result, the substitution kinetics were followed at a constant pH of 4.0 to avoid complication from an additional parameter of $[H^+]$ in the rate equation. To study the effects of temperature, the reactions were studied at five different temperatures of different [thiol] and the rate constants (k_1 and k_2) of the reactions were calculated for both the steps and are given in Table 3. The activation parameters were calculated from Eyring plots (Fig. 6) (ESI Fig. S21 for L-cys and S22, 23

for N-ac-L-cys) (R_2 for k_1 is 0.9923 and R_2 for k_2 is 0.9855) are given in Table 4 and compared with those for analogous systems involving the substitution in square planar Pt(II) complexes.
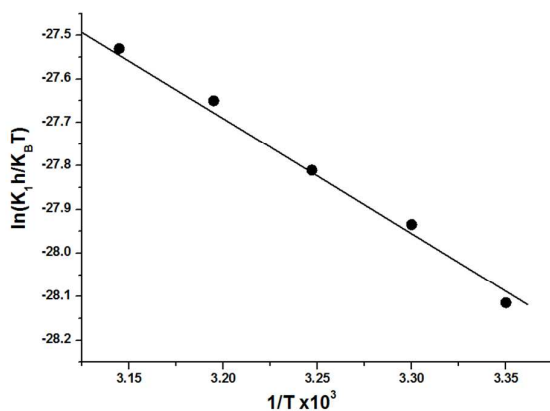
Fig.6 Eyring plot for (ln k_1h/k_BT vs. $10^3 1/T$) of L-cys

Table 4 Activation parameters for analogous systems

Systems	$\Delta H_1^{\ddagger}$	$\Delta S_1^{\ddagger}$	$\Delta H_2^{\ddagger}$	$\Delta S_2^{\pm}$	Ref.
[Pt(MAMP)(H$_2$O)$_2$]$^{2+}$ /L-cys	25.00± 1.35	-207.40 ±1.19	23.34 ±1.14	-253.88±1.65	This work
[Pt(MAMP)(H$_2$O)$_2$]$^{2+}$ /N-ac-L-cys	20.25± 1.46	-229.41 ±1.13	18.22 ±1.17	-272.02±1.81	This work
[Pt(pic)(H$_2$O)$_2$]$^{2+}$ /L-cys	34.91± 0.97	-174.68 ±2.81	29.11 ±0.72	-233.74±2.40	20
[Pt(pic)(H$_2$O)$_2$]$^{2+}$ /N-ac-L-cys	21.12± 0.35	-294.25 ±1.05	19.45 ±0.47	-267.68±1.60	20

Mechanism:

Based on kinetic data (k_1, k_2 and K_E values), low value of enthalpy of activation parameters ($\Delta H_1^{\ddagger}$ and $\Delta H_2^{\ddagger}$) and high negative values of entropy of activation ($\Delta S_1^{\ddagger}$ and $\Delta S_2^{\ddagger}$), the associative mechanism is proposed (Scheme 2) for both the ligand substitution reactions, which are also supported by Job's experiments (1 : 1 metal ligand ratio). Low $\Delta H_1^{\ddagger}$ and high negative $\Delta S_1^{\ddagger}$ values were found from the Eyring plot. Furthermore, the $k_{2(obs)}$ values of second step of the reaction are independent of [thiol], which clearly indicates that it must be the cyclisation process through carboxylate oxygen. Repetitive scan of UV-Vis spectrum shows two distinct isosbestic points, which clearly indicates that the complex **2** is transformed to complex **3** through the formation of intermediate B. The transformation phase from A→B→C is shown in Fig. 3. The plausible mechanism for the interaction of complex **2** with L-cys and N-ac-L-cys is shown as follows.
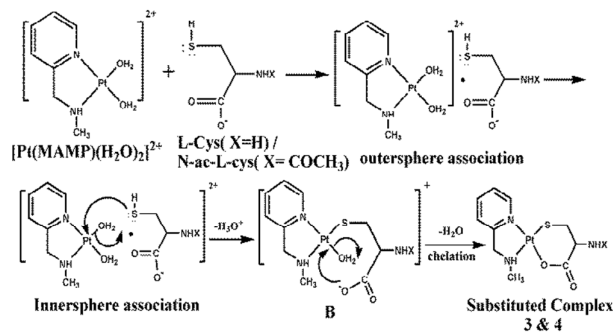
Scheme 2 Plausible mechanism of the reactions between complex **2** with the thiols (L-cys and N-ac-L-cys)

DFT calculations

DFT calculations were performed to optimize the structure of complexes **2-4** to get an insight into the bonding properties of the complexes. The energies of HOMO and LUMO for the complexes **2-4** were calculated from their energies (eV) and surface plots, generated using Gauss view 5.0 shown in Fig. 7. A relationship to some extent between the HOMO–LUMO energy gap of the complexes and their chemical reactivity is expected. Positive and negative regions are shown in red and green colours respectively. Reactivity of complex **2** is related to chemical hardness, which is defined as the resistance to perturb the electron distribution within the complex. The structural parameters bond distances (Å) and bond angles (°) are compared with the observed[52-54] values and shown in table 5.

HOMO -14.6629 e.V	-5.4110 e.V	-4.9122 e.V
Energy gap 4.8014 e.V	3.7127 e.V	2.7113 e.V
LUMO -9.8615 e.V	-1.6982 e.V	-2.2008 e.V
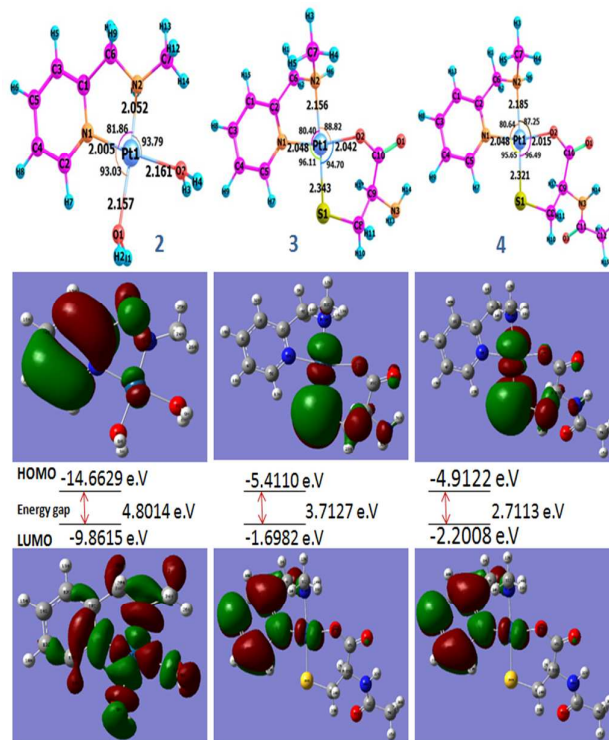
Fig.7 Optimized structures of complexes **2-4** and corresponding counter plots of HOMO, LUMO molecular orbitals

Table 5 Selected bond distances (Å) and bond angles (°) of complex **2-4** calculated from optimized structures

bonds	bond distance (Å)			
	complex **2**	complex **3**	complex **4**	observed
Pt-N1	2.005	2.048	2.048	2.030
Pt-N2	2.052	2.156	2.185	2.039
Pt-S1	-	2.343	2.321	2.356
Pt-O2(thiol)	-	2.042	2.015	2.055
Bond angles	**Bond angles(°)**			
N1-Pt-N2	81.86	80.40	80.64	-
N2-Pt-O2	93.79	-	-	-
N1-Pt-O1	93.03	-	-	-
N2-Pt-O2(thiol)	-	88.82	87.25	-
N1-Pt-S1	-	96.11	95.65	-

Natural Bond Orbital (NBO) analysis

The ligands (L-cys and N-ac-L-cys) have three potential donor centres (S, O and N) to substitute the water molecules from complex **2**. To confirm the bonding mode of ligands with complex **2** NBO analyses was performed. This provides detailed insight into the nature of electronic structure and bonding in the probable complex formation of complex **2** with L-cys/ N-ac-L-cys by considering different donor centres either through (S,O) or (S, N) in the substitution reactions. The complex formation **3** was merely confirmed through (S, O) by considering the charge transfer from donor centre(S,O) to Pt(II). Calculated atomic charge and electronic configurations of donor (S,O) or (S,N) and Pt(II) centre atoms of complex **3**(S,O) and the probable complex **3′**(S,N) are listed in Table 6.

Electron population on s and p orbitals of sulfur, oxygen and nitrogen donor atoms in different probable complexes of **3**, through (S,O) and (S,N) donor are less than the expected values of valence orbitals, while the computed electron population in Pt(II) in both probable complexes of **3**(S,O) and **3′**(S,N) is more than the expected value in Pt(II) with d^8 electronic configuration. The calculated formal charge on Pt(II) ion in complex **3** is lower than the formal charge +2, confirming a significant charge donation from the ligand. The calculated electronic configurations of the donor atoms with reference to s and p orbitals are consistent with electron donation towards the Pt(II) ion. The amount of electron charge density on S is almost same in both the probable complex **3** and **3′** whereas that on O (-0.67489 a. u) is less in complex **3**(S,O) compared to the charge on N (-0.80357a. u) in **3′**(S,N), which indicates the charge transfer from ligand(S,O) to metal is favourable than probable (S,N)donor centre. This theoretical result strongly supports the (S,O) coordination for L-cys with complex **2**. Similar calculation was carried out for complex **4** through (S,O) and (S,N) donor centres (ESI Table S2) which shows the comparable results.

Molecular docking with B-DNA

Molecular docking studies were carried out to obtain a theoretical insight into the interaction between complex **2** and B-DNA (PDB ID: 1BNA) using HEX 8.0.0 software.[55] The docked model[56] results suggest that platinum complex **2** binds with the minor groove of the B-DNA (Fig. 8). The complex **2** forms two hydrogen bonds with the two guanines (1.8 & 2.6 Å) through pyridine nitrogen and one hydrogen bond with water (3.0 Å) of the 30 to 50 polynucleotide chains in B-DNA and total free energy of binding is -14.39 kcal.mol^{-1}. The almost planar structure of the complex fits into the minor groove of the DNA in a parallel manner with respect to the DNA backbone.

Table 6: Charges (a.u.) and electron configurations for the complexes 3(S,O) and 3(S,N)

	Complex 3(S,O)		Complex 3′(S,N)	
Atom	Charge	Natural electronic configuration	Charge	Natural electronic configuration
Pt	0.32732	[core]6S(0.58)5d(8.74)6p(0.33)6d(0.01)7p(0.01)	0.26917	[core]6S(0.57)5d(8.79)6p(0.35)6d(0.02)7p(0.01)
N6	-0.43379	[core]2S(1.28)2p(4.13)3p(0.01)	-0.43422	[core]2S(1.27)2p(4.15)3p(0.01)
N8	-0.65255	[core]2S(1.35)2p(4.29)3p(0.01)	-0.65147	[core]2S(1.34)2p(4.30)3p(0.01)
S20	-0.15342	[core]3S(1.72)3p(4.41)3d(0.01)4p(0.01)	-0.14416	[core]3S(1.73)3p(4.39)3d(0.01)4p(0.01)
O27	-0.67489	[core]2S(1.66)2p(5.00)3p(0.01)	-0.75664	[core]2S(1.77)2p(4.98)
N28	-0.89964	[core]2S(1.43)2p(4.45)3p(0.01)3d(0.01)	-0.80357	[core]2S(1.37)2p(4.41)3p(0.01)

10

Fig. 8 Computational docking model (using HEX Software) of interaction between 2 and B-DNA (PDB ID: 1BNA). Magnified view of the interaction between 2 and DNA

Microscopic observation. HeLa cells were treated with 10 μM of cisplatin and complexes **2–4** were incubated for 12 h to detect cellular survival. The treated and untreated cell debris were washed thrice with PBS and viewed under a light microscope (Zeiss). Survived HeLa cells are shown in Fig. 9. The same experiment was also done with Hep G2 cells which reveal almost similar results (See ESI Fig. 24).
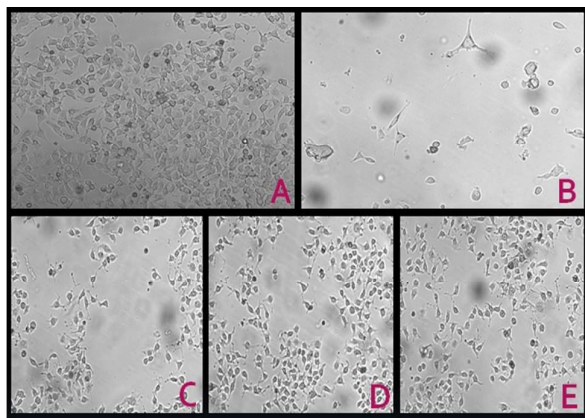
Fig. 9 Morphological changes of cell death for HeLa: (A) cells treated without any complex; (B) with 10 μM of cisplatin; (C) treated with 10 μM of complex 2; (D) 10 μM of complex 3 and (E) 10 μM of complex 4 for 12 h.

DNA interaction studies with the complexes 2 to 4 by agarose gel electrophoresis

To observe the DNA binding and degradation property of Pt(II) complexes, plasmid DNA was incubated with complexes **2–4**. The control was maintained without treating with any of the complexes and electrophoretically run in the 0.8% agarose gel and the band pattern was observed. Mobility of plasmid DNA in lanes 2–4 for complex **2-4** respectively is degraded compared to lane-1 (control DNA). This result suggests that the complex **2-4** have binding affinity to plasmid DNA (Fig. 10).
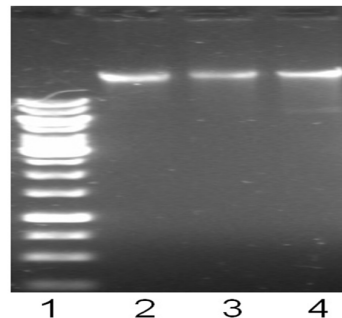
Fig. 10 0.8% agarose gel electrophoresis pattern of the pC DNA3. Lane 1 is control not treated with any complex. Lanes 2 to 4 are DNA treated with complex **2-4** in 5.0 μM concentration

In vitro antibacterial activity

The Pt(II) complexes **2-4** exhibit the antibacterial property on Gram positive and gram negative bacteria. The results of in vitro antibacterial activities of complexes **2-4** are shown in graphs. The rate of growth inhibition of both kinds of bacteria is proportional to the concentration of the complexes in the media. Substituted complex **3** and **4** do not show better inhibition compared to complex **2** alone. Gram negative Escherichia coli show comparatively less inhibition (ESI Fig. S25) than Gram positive Bacillus.subtilis bacteria (ESI Fig. S26). Bacterial infection may also increase the risk of cancer, as seen in *Helicobacter pylori*-induced carcinoma.[57,58] Prior *C. Pneumoniae* infection[59] has been associated with slightly increased risk of developing lung cancer. Since complexes **2-4** possess antibacterial property it may have an added advantage in cases where malignancy is induced by bacterial infections.

In vitro cytotoxicity assay

MTT assay was carried out for anticancer property of complexes **2–4**. The viability of HeLa and Hep G2 cell lines were analyzed within the plates and compared with the control. As shown in Fig. 11 and 12, with increase in the concentrations of the complexes **2-4** the percentage of cell survival of HeLa and Hep G2 cell lines follow a descending trend after 48 h incubation period. These results of in vitro chemo sensitivity evaluation of the cytotoxicity of complexes **2–4** indicate that the cells were not actively proliferating in presence of complexes. The concentration variations of complexes **2-4** were studied from 5 μM to 50 μM.
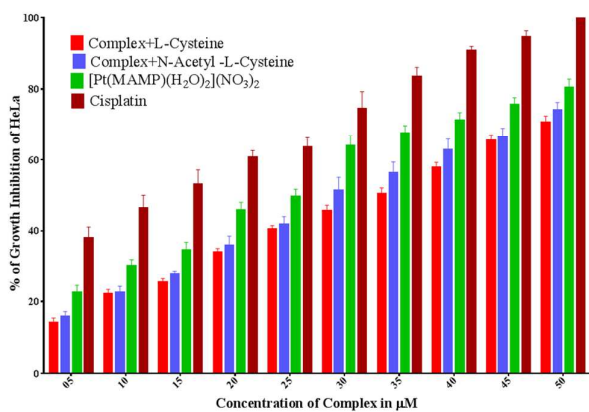
Fig.11 % of growth Inhibition of HeLa cell in presence of [Pt(MAMP)(H$_2$O)$_2$](NO$_3$)$_2$ and complex **3-4** with concentration variation from 5 μM to 50 μM compared to cisplatin
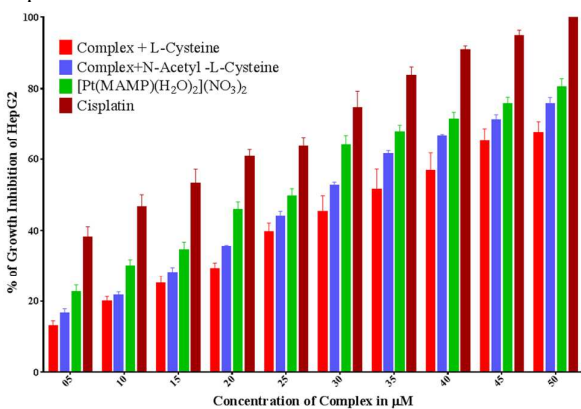
Fig.12 % of growth Inhibition of Hep G2 cell in presence of [Pt(MAMP)(H$_2$O)$_2$](NO$_3$)$_2$ and its L-cys & N-ac-L-cys substituted complexes **3-4** from 5 μM to 50 μM concentrations compared to cisplatin

The complex **2** has better anticancer property than thiol substituted Pt-S complex **3-4** as shown in Fig. 11 and 12. It may be explained by considering the SHAB principle in both the cases of complex **2** and **3-4**. According to this principle Pt-S bonds are less labile than Pt-OH$_2$ and interaction of the complex **2** with DNA is more favourable than Pt-S bonded complex **3-4** for Pt-DNA adduct formation. Consequently, anticancer property of complex **2** is quite better than Pt-S complexes.

Conclusion

Pt(II) complexes **2-4** were synthesised and characterised spectroscopically and their bioactivity like anticancer, antibacterial and DNA binding properties were investigated. Sulfur containing bio-relevant ligands L-cys and N-ac-L-cys have high affinity towards complex **2** and represent a model reaction as 'drug reservoir'. In complex **2**, σ donor and π-acceptor carrier ligand MAMP has a secondary amine group(-NHCH$_3$), which has direct influences on the reactivity as well as bioactivity. Formation of complex **3** and **4** with the respective thiol via (S, O) chelation is confirmed by theoretical investigation, which is in

good agreement with NBO analysis. Activation parameters, enthalpy ($\Delta H_1^\ddagger$ and $\Delta H_2^\ddagger$) and entropy ($\Delta S_1^\ddagger$ & $\Delta S_2^\ddagger$) for both reactions are found low and negative respectively for the first and second steps of substitution processes, which suggests an associative mode of activation for their transition states(T.S). The activation parameters also imply a good degree of ligand participation in associative path of the T. S.

DFT calculations were carried out for global minimum optimized structures of complex **2-4**, which reveals few important bond distances (Å) and bond angles (°) close to the reported values. HOMO and LUMO calculation of complex **2** shows that electron density of HOMO is localized mostly on pyridine ring of carrier ligand MAMP and minimum on the metal ion without significant contributions, whereas in case of LUMO major contributions are from the metal ion. Electron transfer occurs from the HOMO to LUMO in complex **2** is related to LMCT. But the charge density of HOMO for complex **3** and **4** is localised on L-cys and N-ac-L-cys part of the complex respectively, whereas LUMO is localised on MAMP, suggesting a LLCT transition for **3** and **4**. NBO analysis reveals the (S,O) coordination rather than (S,N) for both the complex **3** and **4**.

Complexes **2–4** have significant anticancer and antibacterial properties. The complexes have shown notable growth inhibition on gram positive and gram negative bacteria. In vitro cytotoxicity evaluation by MTT assay of complexes indicates that HeLa and Hep G2 cells were not actively proliferating in presence of Pt(II) complexes **2-4**. Complex **2** shows better anticancer activity than complexes **3-4.** Its activity is about 70–75% on both HeLa and Hep G2 cell lines at higher concentration (50 μM) compared to cisplatin, which is remarkable. The molecular docking suggests that the almost planar structure of the complex **2** fits into the minor groove of B-DNA in a parallel manner with respect to the DNA backbone. A mechanistic understanding of biomolecular interaction and DNA binding will provide a rational basis for the design of new platinum based anticancer agents with reduced toxicity and high specificity. Further insight into their physiological processing and pharmacological effects will be beneficial for the development of these Pt complexes as therapeutics.

Acknowledgements

Reference
1 B. Rosenberg, L. Vancamp and T. Krigas, *Nature*, 1965, **205**, 698.

RSC Advances Accepted Manuscript

2 B. Lippert, *Cisplatin: chemistry and biochemistry of a leading anticancer drug. Wiley*, Zu¨rich, 1999.

3 B. Rosenberg, L.V. Camp, J. E. Trosko and V. H. Mansour, *Nature*, 1969, **222**, 385.

4 E. Wong and C. M. Giandomenico, *Chem. Rev.* 1999**, 99**, 2451.

5 R. B. Weiss and M. C. Christian, *Drugs,* 1993, **46**, 360.

6 B. Rosenberg, In *Cisplatin:Chemistry and Biochemistry of a Leading Anticancer Drug;* Ed. B. Lippert, Verlag Helv. Chim. Acta. Zurich; Wiley-VCH: Weinheim, Germany, 1999; 3.

7 P. J. O'Dwyer, J. P. Stevenson and S. W. Johnson, *Cisplatin: Chemistry and Biochemistry of a Leading Anticancer Drug,* Ed. B. Lippert, Verlag Helvetica Chimica Acta: Zurich; Wiley-VCH: Weinheim, Germany, 1999, **31**.

8 T. Niioka, T. Uno, N. Yasui-Furukori, T. Takahata, M. Shimizu, K. Sugawara and T. Tateishi, *Cancer Chemother Pharmacol*, 2007, **59(5)**, 575.

9 D. Lebwohl and R. Canetta, *Eur. J. Cancer,* 1998**, 34***, 1522.

10 I. Judson and L. R. Kelland, *Drugs,* 2000, *Suppl* **59**, 29.

11 S. Wimmer, P. Castan, F L. Wimmer & N P. Johnson, *J. Chem Soc, Dalton Trans*, 1989, **403**.

12 J. Reedijik, *Chem. Rev.,* 1999, **99**, 2499.

13 A. Bart, J. Jansen, J. Brouwer and J. Reedijk, *J. Inorg. Biochem.*, 2002, **89**, 197.

14 M. A. Jakupec, M. Galanski and B. K. Keppler, *Rev. Physiol., Biochem. Pharmacol*, 2003, **146**, 1.

15 J. Reedijk, *Eur. J. Inorg. Chem.*, 2009, **10**, 1303.

16 T. Soldatovi´c and ˇZ. D. Bugarˇci´c, *J. Inorg. Biochem.*, 2005, **99**, 1472.

17 X. Wang and Z. Guo, *Anti-Cancer Agents in Med. Chem.,* 2007, **7**, 19.

18 D. Živadin, Bugarčič, G. Liehr and R. Van Eldik, *Chem. Soc., Dalton Trans.* 2002, 2825.

19 M. Noji, K. Okamoto, T. Tashiro and Y. Kidani, *J. Med. Chem.*, 1981, **24(5)**, 508.

20 A. Samanta, G. K. Ghosh, I. Mitra, S. Mukherjee, W. Linert, B. Misini, J.C. Bose K, S. Mukhopadhyay and S. C. Moi, *RSC Adv.*, 2014, **4**, 43516**.**

21 K. Misra, G. K. Ghosh, I. Mitra,   S. Mukherjee, V. P. Reddy B., W.Linert, B.Misini ,   J. C. Bose K, S. Mukhopadhyay and S. C. Moi, *RSC Adv.,* 2015**, 5**, 12454**.**

22 A. D. Becke, *J. Chem. Phys.* 1993, **98**, 5648.

23 C. Lee, W. Yang and R.G. Parr, *Phys. Rev. B,* 1988, **37**, 785.

24 M. J. Frisch, G. W. Trucks, H. B. Schlegel, G. E. Scuseria, M. A. Robb, J. R. Cheeseman, G. Scalmani, V. Barone, B. Mennucci, G. A. Petersson, H. Nakatsuji, M. Caricato, X. Li, H. P. Hratchian, A. F. Izmaylov, J. Bloino, G. Zheng, J. L. Sonnenberg, M. Hada, M. Ehara, K. Toyota, R. Fukuda, J. Hasegawa, M. Ishida, T. Nakajima, Y. Honda, O. Kitao, H. Nakai, T. Vreven, J. A. Montgomery, Jr., J. E. Peralta, F. Ogliaro, M. Bearpark, J. J. Heyd, E. Brothers, K. N. Kudin, V. N. Staroverov, R. Kobayashi, J. Normand, K. Raghavachari, A. Rendell, J. C. Burant, S. S. Iyengar, J. Tomasi, M. Cossi, N. Rega, J. M. Millam, M. Klene, J. E. Knox, J. B. Cross, V. Bakken, C. Adamo, J. Jaramillo, R. Gomperts, R. E. Stratmann, O. Yazyev, A. J. Austin, R. Cammi, C. Pomelli, J. W. Ochterski, R. L. Martin, K. Morokuma, V. G. Zakrzewski, G. A. Voth, P. Salvador, J. J. Dannenberg, S. Dapprich, A. D. Daniels, Ö. Farkas, J. B. Foresman, J. V. Ortiz, J. Cioslowski, and D. J. Fox, Gaussian, Inc., Wallingford CT, 2009, Gaussian 09, Revision D.01.

25 P. J. Hay and W. R. Wadt, *J. Chem. Phys.,* 1985, **82**, 299.

26 P. J. Hay and W. R. Wadt, *J. Chem. Phys.,* 1985, **82**, 284.

27 R. Ditchfield, W. J. Hehre and J. A. Pople, *J. Chem. Phys.,*1971, **54**, 724.

28 W. Hehre, J. R. Ditchfield and J. A. Pople, *J. Chem. Phys.,* 1972, **56**, 2257.

29 E. D. Glendening, A. E. Reed, J. E. Carpenter and F. Weinhold, NBO Version 3.1.

30 R. W. Hay and A. K. Basak, *J. Chem. Soc., Dalton Trans.,* 1982, 1819.

31 S. Hochreuther, R. Puchta and R. van Eldik, *Inorg. Chem.* 2011, **50**, 8984.

32 J. A. Weyh and R. E. Hamm, *Inorg. Chem.*, 1969, **8**, 2298.

33 R. I. Freshney, *Culture of animal cells: A manual of basic technique, Wiley-Liss, NY, 5th edn*, 1987, p. 200.

34 R. W. Masters, *Animal cell culture: Cytotoxicity and viability assays, 3rd edn*, 2000, **23**, 202.

35 D. Garmann, et al., *J. Controlled Release*, 2008, **131**, 100.

36 Y. C. Sasaki and A. Passaniti, *BioTechniques*, 1998, **24**, 1038.

37 Th. Z. Huyskens, P. Huyskens, H. Ratajczak, W. J. Orville-Thomas, *Molecular Interactions (Russian Edition), Mir, Moscow*, 1984, 17.

38 L. Tian, B. Zhao, Z. Zhou, Q. Yu and W. Yu, *Synth. React. Inorg. Met.-Org. Chem.*, 2002, **32**, 939.

39 (a) J. L. Tian, E. Q. Gao, Y. T. Li and S. X. Liu, *Synth. React. Inorg. Met.Org. Chem.*, 1995, **25**, 417; (b) S. Liu, J. Tian, E. Gao, S. Bi and Y. Li, *Synth. Inorg. Met.Org. Chem.,* 1996, **26**, 1447.

40 (a) J. H. Price, A. N. Williamson, R. E. Schramm and B. B. Wayland, *Inorg. Chem.*, 1972, **11**, 1280; (b) N. I. Dodoff, D. K. Demertzi, M. Kubiak, J. K. Jaworskac, A. Kochel and G. A. Gorneva, *Z. Naturforsch., B: J. Chem. Sci.,* 2006, **61**, 1110.

41 M. Chandrasekharan, M. R. Udupa and G. Aravamudan, *Inorg. Chim. Acta*, 1973, **7**, 88.

42 K. Nakamoto, *IR and Raman Spectra of Ing. and Coord. Comp., Part B, J. Wiley and Sons, New York,* **5th edn**.,1997.

43 J. Fujita, A. E. Martell and K. Nakamotom, *J. Chem. Phys.,* 1962, **36**, 324.

44 G. T. Behnko and K. Nakamoto, *Inorg. Chem.,* 1968, **7**, 2030.

45 R. A. Condrate and K. Nakamoto, *J. Chem. Phys.*, 1965, **42**, 2590.

46 R. M. Smith and A. E. Marttu, *Critical Stability Constants, Plenim Press, NewYork*, 1989, 21.

47 T. M. Hui and T. C. Thou, *AAPS J.,* 2006, **8**, 485.

48 P. Karmakar, S. Mallick, B. K. Bera, A. Mandal, S. Mondal, S. K. Mukhopadhyay and A. K. Ghosh, *Transition Met. Chem.*, 2010, **35**, 911.

49 P. Karmakar, B. K. Bera, K. L. Barik, S. Mukhopadhay and A. K. Ghosh, *J. Coord. Chem.*, 2010, **63**, 2158.

50 W. Shen, R. D. Schnebeck, E. Freisinger and B. Lippert, *Dalton Trans.*, 2008, 4044.

51 K. Sakai, Y. Konno, N. Takayama and S. Takahashi, *Acta Crystallogr., Sect. B: Struct. Sci., Cryst. Eng. Mater.*, 2004, **60**, 255.

52 W. Z. Shen, R. D. Schnebeck, E. Freisinger and B. Lippert, *Dalton Trans.*, 2008, 4044

53 E. Colacio, R. Cuesta, M. Ghazi, M. A. Huertas, J. M. Moreno, and A. Navarrete, *Inorg. Chem.* 1997, *36,* 1652

54 R. Wysokin´ ski, K. Hernik, R. Szostak and D. Michalska, *Chemical Physics,* 2007, **333**, 37.

55 G. Macindoe, L. Mavridis, V. Venkatraman, M. D. Devignes and D. W. Ritchie, Hex Server: an FFT-based protein docking server powered by graphics processors, Nucleic,Acids Res., 2010, 38, DOI: 10.1093/nar/gkq311, Pub Med PMID: 20444869; Pub Med Central PMCID: PMC2896144.

56 K. Suntharalingam, O. Mendoza, A. Alexandra Duarte, D. J. Mann and R. Vilar, *Metallomics*, 2013, **5**, 514.

57 S. Peter and C. Beglinger, *Digestion*, 2007, **75(1)**, 25.

58 C. Wang, Y. Yuan and R.H. Hunt, *Am. J. Gastroenterol.*, 2007, **120(8)**, 1789.

59 P. Zhan, L. J. Suo and Q. Qian, *Eur. J. Cancer*, 2011, **47(5)**, 742-747.